Landscape Ecol (2012) 27:529–543
DOI 10.1007/s10980-012-9703-x

RESEARCH ARTICLE

Detection of relative differences in phenology of forest species using Landsat and MODIS

Bernard N. Isaacson · Shawn P. Serbin · Philip A. Townsend

Received: 11 March 2011 / Accepted: 1 January 2012 / Published online: 10 January 2012

Abstract Landsat imagery is routinely used to characterize stand-level forest communities, but low temporal resolution makes pixel-wise characterization of phenology difficult. This limitation can be overcome by using multi-year imagery, but organizing Landsat scenes by calendar date ignores phenological gradients across the landscape as well as inter-annual differences in both scene- and pixel-wise phenology. We demonstrate how a spatially generalizable, phenologically-informed approach for re-ordering Landsat pixels can be used to characterize spatial variations in autumn senescence in several forest tree species. Using end-of-season estimates derived from MODIS phenology data, we determined the "days left in season" (DLiS) across Landsat images to produce a synthesized phenological trajectory of the normalized difference infrared index (NDII). We used ground-based species composition data in conjunction with the NDII trajectories to model autumn senescence by species. Absolute phenology differed by one and a half to 3 weeks between northern and southern Wisconsin, USA, but we show that the relative timing of phenology for individual species differs across regions by only 1–3 days when considering senescence with respect to the local end of the season. The progression of species senescence was consistent in lowland stands, starting with green and black ash, followed by silver maple, yellow birch, red maple, and tamarack. The image analyses suggest that senescence progressed more rapidly in southern than northern Wisconsin, starting earlier but taking about ten more days in the north. Our results support the use of MODIS phenological data with multi-year Landsat imagery to detect species with unique phenologies and identify how these vary across the landscape.

Keywords Vegetation phenology · Landsat · MODIS · Forest · Autumn

Introduction

The behavior of vegetation communities varies across landscapes according to differences in environmental drivers (Jolly et al. 2005; Richardson et al. 2006). One response to these environmental variations is differing phenologies both within and between species (Lechowicz 1984; Hwang et al. 2011), although the range of response within a single species may be greater than observed abiotic variability (Liang and Schwartz 2009). Phenological variability among species has long been used to discriminate patterns of species

Electronic supplementary material The online version of this article (doi:10.1007/s10980-012-9703-x) contains supplementary material, which is available to authorized users.

B. N. Isaacson (✉) · S. P. Serbin · P. A. Townsend
Department of Forest and Wildlife Ecology, University of Wisconsin—Madison, 226 Russell Laboratories, 1630 Linden Drive, Madison, WI 53706, USA
e-mail: bernardisaacson@gmail.com; bisaacson@wisc.edu

composition using well-timed remote sensing data (Wolter et al. 1995; Dymond et al. 2002). However, climatic differences between disconnected landscapes inhabited by the same species limit the ability to generalize the phenology for a given vegetation type within the region covered by the remote sensing data.

High spectral resolution imagery has been used for species mapping over small areas (Martin et al. 1998; Williams and Hunt 2002; Kokaly et al. 2003), while moderate spatial resolution sensors such as Landsat are more commonly used for mapping community types or locally dominant species (Wolter et al. 1995; Townsend and Walsh 2001) over broad extents. Previous studies have utilized phenological state within well-timed image sets to classify forest types (Wolter et al. 1995; Mickelson et al. 1998; Townsend and Walsh 2001; Dymond et al. 2002). Although knowledge of species phenology has been shown to improve forest classification accuracy, the 15-day revisit interval of Landsat sensors makes them poorly suited to characterize discrete phenological events within a single year (Kodani et al. 2002). This is because the timing of particular phenological events shifts slightly from year to year due to inter-annual differences in climate (Lee et al. 2003). Nevertheless, there is consistency in the relative order of events from year-to-year among species in a plant community (Leopold and Jones 1947; Lee et al. 2003).

However, since phenology varies spatially, Landsat image pairs may not (and often, do not) capture specific phenological events, or do not do so across their entirety. Even if phenology can be quantitatively characterized in one Landsat footprint with a set of scenes at ideal calendar dates, phenological relationships cannot necessarily be extended to adjacent scenes with non-ideal image pairs. Within- and across-scene phenological gradients, as well as the absence of well-timed or cloud-free images, prohibit the extension of relationships across scenes. In contrast, multiple years of Landsat imagery have been used to characterize the phenology of a pixel at the Landsat scale (Fisher et al. 2006). We feel that to identify species using methods similar to Fisher et al. (2006), it is extremely important to account for differences in phenology as a consequence of interannual climate variability and spatial gradients.

We examine numerous species in this study, but focus primarily on ash species (*Fraxinus* spp.). Ash trees exhibit a unique phenology that makes them a useful test taxon. In the upper Midwestern US, ashes are among the last trees to leaf out in spring and first to drop their leaves in the autumn (Ahlgren 1957; Lechowicz 1984; Knutson 1997). Ashes' autumn leaf phenology has been used previously to discriminate dense communities of black ash (*F. nigra*) in forest type mapping (Wolter et al. 1995). Ashes are also of interest because they currently are threatened by the emerald ash borer (EAB, *Agrilus planipennis*, Haack et al. 2002), making the detection of ash an important management objective. The research presented here provides the foundation for the eventual mapping of ash abundance through the observation of landscape phenological patterns using multi-sensor remote sensing data.

Here we demonstrate an approach for species characterization that considers the inherent temporal and spatial variability of phenology across a landscape. Our methods allow us to describe the contrasting phenology of individual species within Landsat pixels in a consistent manner along phenological gradients among landscapes in northern and southern Wisconsin. We believe that our methods will facilitate future efforts to confidently map the abundance of phenologically-unique species at a regional spatial extent.

Methods

Our approach for characterizing phenology by species across climatic gradients incorporates ground-based data, a rich Landsat time series, and MODIS phenology products. The calendar-date timing of Landsat data are standardized using the MODIS products, and vegetation indices from the date-standardized Landsat data are then used with the ground data to perform analyses of species phenology across the landscape.

Ground-based forest composition data collection

Forest composition data were collected between May 2008 and September 2009, in and around the Flambeau River State Forest (FRSF) in northern Wisconsin ($n = 49$ sample plots), and Kettle Moraine State Forest (KMSF) in southern Wisconsin ($n = 99$) (Fig. 1). We sampled mesic, dry-mesic, and wet-mesic southern and northern hardwoods, as well as wet and wet-mesic northern forest (Tables 1, 2) (Curtis 1959). Weather stations near FRSF show mean January temperature of

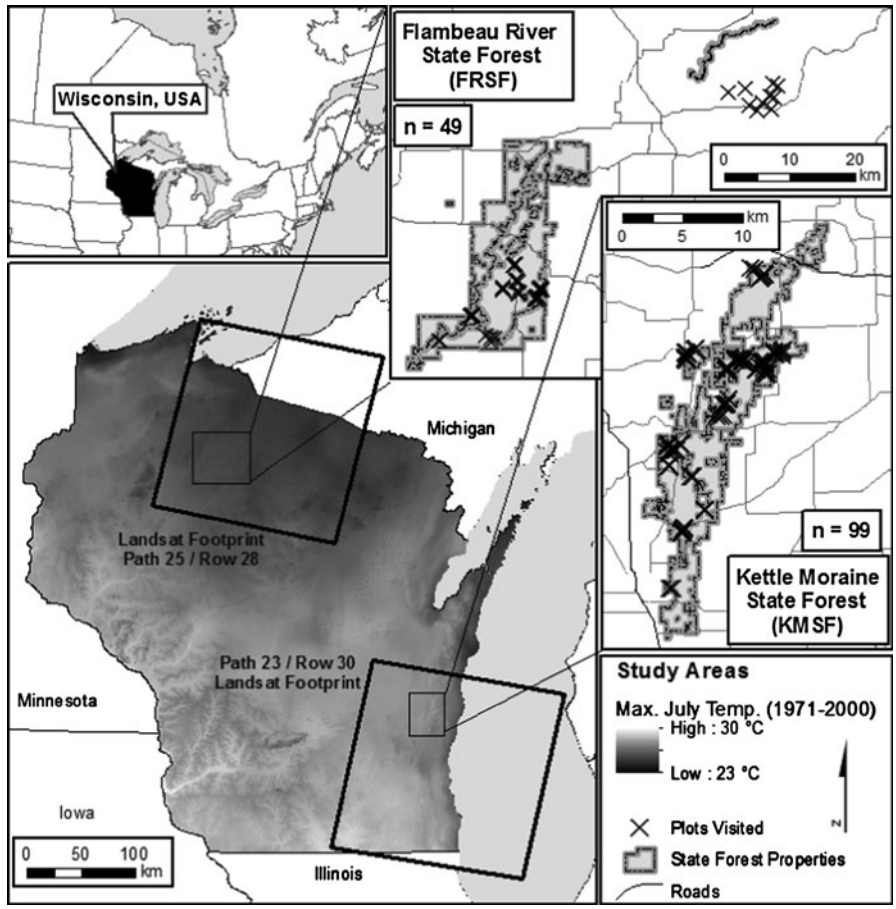

Fig. 1 Study areas in Wisconsin demonstrating climatic variability. Climate data: PRISM Climate Group, Oregon State University, http://www.prismclimate.org, created 4 Feb 2004

Table 1 Species-wise field data collected in Kettle Moraine State Forest, southern Wisconsin (ground plot $n = 99$, '*n* obs.' column represents number of plots on which species was found)

Species	Common name	*n* Obs.	Max. observed % of basal area	*n* Above 50% of basal area
Fraxinus nigra	Black ash	35	78.3	7
F. americana	White ash	47	41.4	0
F. pennsylvanica	Green ash	39	91.0	9
Acer rubrum	Red maple	52	64.9	1
A. saccharinum	Silver maple	8	80.9	1
A. saccharum	Sugar maple	66	63.0	2
Carya ovata	Shagbark hickory	47	49.1	0
Populus tremuloides	Trembling aspen	18	36.5	0
P. grandidentata	Bigtooth aspen	25	44.9	0
Quercus alba	White oak	42	23.8	0
Q. rubra	Red oak	61	57.8	3
Tilia americana	American basswood	51	27.4	0
Ulmus americana	American elm	55	34.2	0

−13.4°C and mean July temperature of 19.3°C. KMSF is approximately 5°C warmer in January and 2°C warmer in July. In addition, KMSF experiences an average of 2,769 accumulated modified growing degree days (GDD, base 10°C, ceiling 30°C), or 'thermal accumulation units (in units of °C),' over the

Table 2 Species-wise field data collected in Flambeau River State Forest, northern Wisconsin (ground plot $n = 49$, 'n obs.' column represents number of plots on which species was found)

Species	Common name	n Obs.	Max. observed % of basal area	n Above 50% of basal area
Fraxinus nigra	Black ash	25	91.8	11
F. americana	White ash	16	34.9	0
Acer rubrum	Red maple	36	53.1	1
A. saccharum	Sugar maple	24	91.3	6
Betula papyrifera	Paper birch	10	50.0	0
B. alleghaniensis	Yellow birch	32	27.9	0
Larix laricina	Tamarack	5	94.4	2
Populus tremuloides	Trembling aspen	14	93.2	3

length of the season, while FRSF experiences 2,134 modified GDD (Young et al. 2007).

Sample locations were selected through visual interpretation of aerial photographs from the National Agricultural Inventory Program (NAIP), along with stand-level data from timber inventories. Each plot consisted of a perpendicular pair of randomly oriented, bisecting 60 m transects; at the intersection and ends, we measured species-wise basal area in a variable-radius plot using a two-factor metric wedge prism, creating five sub-plots. This plot size, twice the dimensions of a Landsat TM pixel, was chosen to ensure that at least one Landsat pixel was fully characterized by the ground area measured (Townsend 2001). Whole-plot composition was calculated from the aggregated sub-plot data, which was then used to calculate species-wise relative basal area by plot. Plot locations were recorded using post-processed differential GPS.

Local senescence measures through landsat data

Landsat images were selected based on their atmospheric clarity (cloudiness, aerosol contamination), seasonal timing (June to November), and age (2001–2007) (Appendices 1, 2). Images were obtained from the USGS Global Visualization Viewer website, the Global Land Cover Facility (GLCF), and the WisconsinView website. We projected all data to a common coordinate system, converted them from radiance to top-of-atmosphere reflectance, and manually masked clouds and cloud-shadows. All images were normalized using histogram matching based on the reflectance of dense conifer plantations, which were the most seasonally stable vegetation type on the landscape, and because they captured the spectral range and variation of interest for the study.

We calculated the pixel-wise Normalized Difference Infrared Index (NDII, Hardisky et al. 1983) as a measure of vegetation phenological condition. Previous studies have shown that indices incorporating short-wave infrared radiation are effective for assessing relative differences in leaf loss from thick canopies (Delbart et al. 2005; Stimson et al. 2005; de Beurs and Townsend 2008), and NDII has been observed to be highly sensitive to foliage water content (Gao 1996). Since it does not utilize visible wavelengths, which are more strongly affected by atmospheric conditions, as well as color variability among species in autumn (Lee et al. 2003), and the NDII does not saturate at moderate canopy thickness level (Gao 1996), we preferred NDII over NDVI to determine autumn senescence. We defined senescence not as the onset or threshold level of leaf coloring, but rather as the reduction in canopy water content resulting from leaf senescence and drop. NDII is calculated as:

$$\mathrm{NDII} = \frac{\rho_{\mathrm{NIR}} - \rho_{\mathrm{SWIR}}}{\rho_{\mathrm{NIR}} + \rho_{\mathrm{SWIR}}} = \frac{\mathrm{TM}_4 - \mathrm{TM}_5}{\mathrm{TM}_4 + \mathrm{TM}_5} \quad (1)$$

where ρ_{NIR} is TM and ETM + band 4 reflectance, and ρ_{SWIR} is TM and ETM + band 5 reflectance.

Regional phenology data from MODIS phenology products

MODIS-based phenology data were obtained from the North American Carbon Program (NACP). NACP data provide pixel-wise (500 m) phenology metrics for a given growing season's length, date of green-up,

end of season (EOS) date, and other parameters for the years 2001–2004, and 2006–2007 (data available at the time of analysis). These parameters are determined from an asymmetric Gaussian model fit to time-series MODIS NDVI data (Morisette 2009). NACP data are processed and distributed by the MODIS for NACP system (http://accweb.nascom.nasa.gov developed under Cooperative Agreement *NNH05ZDA001 N-ACCESS with NASA).* Though it is based on NDVI, we used the NACP phenology product because it is sufficient to characterize broad-scale differences in land-surface phenology needed to place Landsat pixels in their annual phenological context. We used the NACP EOS for all of the years for which NACP data were available, which constricted the range of Landsat images available.

The NACP data were spatially smoothed in MATLAB using a low-pass Weiner filter to reduce fine-scale variability while retaining sharp boundaries in phenology, such as those occurring at the edges of vegetation cover types. This provided local context to the phenological trends in an area, reducing the possibility that the presence of large, monospecific forests would obscure actual multi-species phenological trends. Data gaps caused by pixel resolution differences were filled using the mean of a 7×7 kernel.

Phenological ordering of multi-year landsat pixels, 'Days Left in Season':

Studies have tended to concentrate on spring phenology (Ahl et al. 2006; Delbart et al. 2008), but analysis of autumn phenology provides information on important biological processes such as retranslocation of nutrients, and is especially useful for discrimination of deciduous forest types with unique fall signatures. We introduce "Days Left in Season" (DLiS) as a new measure of phenology to characterize autumn vegetation dynamics in a biologically meaningful way. From the NACP phenological data, we modeled the DLiS for each forested Landsat pixel in each image. We define a Landsat pixel's DLiS as the difference between the date on which the Landsat image was collected and the EOS date obtained from the NACP phenology data for that pixel for that year (Fig. 2). Data from multiple years were then ordered into a range where the end of the growing season is set to zero (2):

$$\begin{aligned}\text{DLiS} = &(\text{day of year of Landsat image}) \\ &- (\text{EOS date from processed NACP}) \end{aligned} \quad (2)$$

DLiS, a representation of absolute phenological position within a standardized growing season, was calculated for each Landsat pixel on the date of each

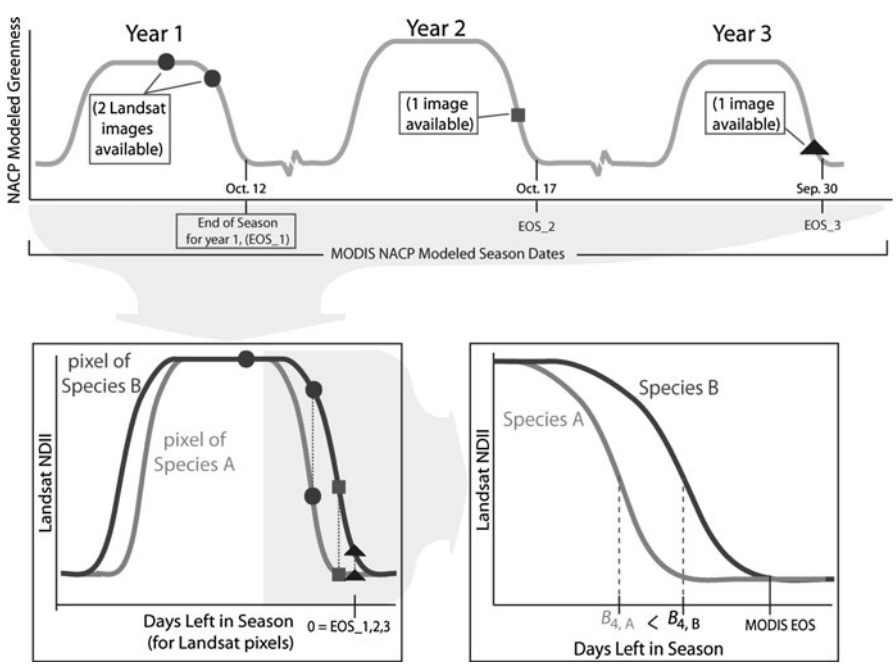

Fig. 2 Pixel-wise phenological re-ordering of Landsat based on annual MODIS end-of-season estimates. B_4 represents the inflection point of the curve, or timing of senescence

Landsat image. All Landsat pixels within a MODIS cell receive the same DLiS. Resolution differences between the Landsat and MODIS data (30 m vs. 500 m) were addressed by sampling the NACP data at the center of each Landsat pixel (nearest-neighbor resampling). The result is a spatial record of phenological timing that is decoupled from the Gregorian calendar and unaffected by interannual and geographic phenological variability.

Species-wise phenology

We extracted NDII and DLiS pixel values for each image date at each field plot location. Using weighted non-linear least-squares regression, we fit NDII (dependent variable) to DLiS (independent variable) to chart the phenology of major species in each area (FRSF or KMSF) (Fig. 3). Each ground plot had been imaged by Landsat 15–25 times over 2001–2007, providing the same number of measurements of NDII and DLiS as available images. We plotted all of these together for a study region, and for each species of interest in that region, we weighted the observations with the relative basal area for that species. Plots with a greater proportion of a species were more influential in modeling the phenology of that species (e.g., Fig. 3). To these data we fit a reverse logistic curve to determine the phenology of each species of interest, where:

$$\mathrm{NDII}(\mathrm{DLiS}) = \beta_1 + \beta_2\left(\frac{1}{1 + e^{\beta_3 * (\beta_4 - \mathrm{DLiS})}}\right) \qquad (3)$$

β_1 was the minimum NDII (i.e., background greenness), β_2 was the amplitude of the NDII observations for the pixel, β_3 represented the slope of the senescence model, β_4 was the position of the inflection point of the curve, and *DLiS* represented the days left in season. A reverse logistic curve was selected because of its wide use to characterize the pattern of autumn leaf drop in temperate deciduous forests (e.g., Dixon 1976). Due to the rapid onset of snow cover at the end of the growing season as well as the quick response of vegetation to snowmelt in the spring, there were few snow-free Landsat images available in the leaf-off portion of the season that could be used to fit the leaf-off NDII minimum. Where seasonal minima data were not available, we supplemented the Landsat data with NDII values from cloud- and snow-free MODIS imagery to ensure sufficient observations to fit the reverse logistic curve.

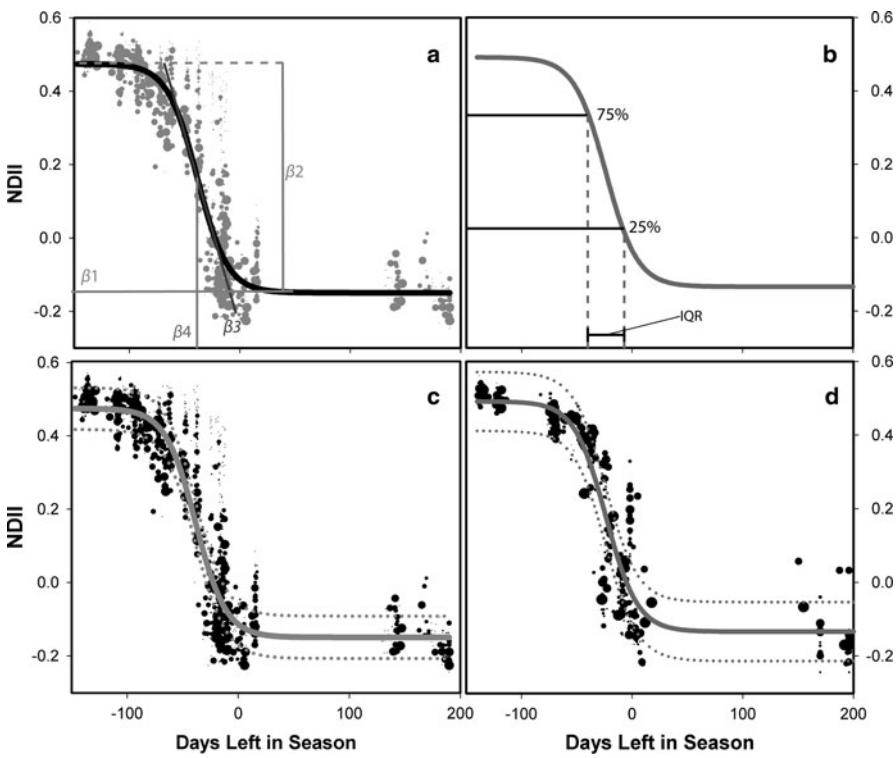

Fig. 3 Curve fitting parameters (**a**), senescence duration (inter-quartile range, IQR) to give biological meaning to slope of curve (**b**), fitted curve for black ash in Kettle Moraine State Forest (**c**), and fitted curve for sugar maple in Flambeau River State Forest (**d**). Broken lines in (**c**) and (**d**) are 95% prediction intervals; each point represents the value for one pixel in one Landsat image covering one ground plot, weighted by the relative basal area of the species of interest

Confidence intervals for the best-fit parameters were obtained through 1,000 bootstrap simulations computed using the "boot" package (Canty and Ripley 2009) in R. These simulated datasets were used to examine model consistency for the same species in different areas. Species-wise comparisons of slopes were conducted via unpaired, two-sided t-tests. We performed a comparison of means test using Tukey's HSD to compare the modeled inflection point of each species in each area (treating the same species in different areas as two separate populations). To give differences in slope biological meaning (i.e., how much longer does it take for the same species to drop its leaves?) we defined a new parameter as the 'inter-quartile range' (IQR). This was the difference (in days) between the DLiS value at 25 and 75% of the maximum NDII value (Fig. 3b); IQR duration for the same species in different areas was compared using paired two-sided *t*-tests.

We also fit phenology models to the data without the DLiS scaling to compare our method against use of calendar date to phenologically order Landsat images across years. For these models, the NACP phenology data were not used; the independent variable value assigned to each Landsat pixel was the day of the year on which the image was acquired. Calendar-date organization is assumed when utilizing image-differencing for species identification, causing images to be treated as phenologically homogenous. While previous work has addressed interannual differences in phenology by using calendar-date organization with an image-wide offset (Fisher et al. 2006), it has been suggested that it is more important to consider spatial differences in phenology (Schwartz et al. 2002; Fisher and Mustard 2007). We compared DLiS to Landsat image calendar date to test whether the method accounted for differences in as well as the interaction between interannual and spatial differences in phenology. Bootstrap simulations following the same procedure were created for this dataset, and were used for comparison to our method.

Results

Our results focus on species that are locally abundant enough on individual plots (i.e. basal area $> 50\%$ of plot BA) to be characterized confidently using imagery. Of the species most commonly found in the southern study area, six had a relative basal area greater than 50% on at least one plot (Table 1). For the northern study area, five species met this criterion (Table 2). Black ash, red maple (*Acer rubrum*), and sugar maple (*A. saccharum*) were abundant in both regions and are used in comparisons between northern and southern Wisconsin. Though it was less abundant than other species in both areas, white ash (*F. americana*) was included in the analysis because of our interest in ash.

Comparisons within species

Black ash exhibits a relatively consistent pattern of senescence between our northern and southern study areas (Fig. 4a). For the duration of senescence, the patterns of senescence track each other, although there is a divergence between their phenologies beginning roughly 30 days prior to the completion of senescence. At this point, black ash in the north exhibit a higher minimum NDII than in the south.

Red maple, white ash, and sugar maple have patterns of senescence that are consistent between north and south (Fig. 4b–d). NDII decline begins later in the south, and senescence is more gradual in the northern site. For each species, prediction intervals for the curves overlap for the duration of senescence (Fig. 4). Summer NDII maxima and winter leaf-off minima for each species are similar in both areas.

For each of the four species examined in both study areas, 95% confidence intervals of the point at which an NDII value of 0.2 is reached do not overlap with the DLiS model, indicating that the timing of senescence is different (Table 3). This trait was selected because it was roughly half of the amplitude for most of the curves, was separate from the inflection point parameter, and was less sensitive to differences in understory composition. Despite significant differences in the timing of passing this threshold, the differences using DLiS are much smaller than the differences obtained from an approach using calendar date. Modeled curves for the same species in different areas show the effect of standardizing via DLiS rather than calendar date (Fig. 5).

The slope (β_3) from the DLiS method for each species in the northern area differs significantly from that obtained in the southern area (Table 4). Slope is 30–35% more gradual in northern Wisconsin for each of the four species modeled, suggesting that

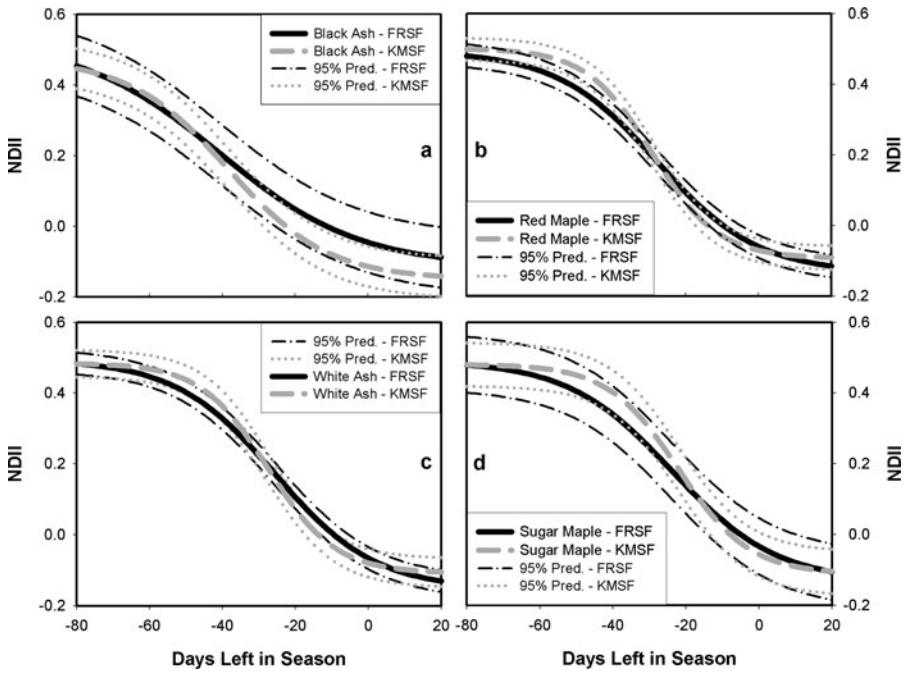

Fig. 4 Modeled curves and 95% prediction intervals for **a** black ash, **b** red maple, **c** white ash and **d** sugar maple in Kettle Moraine State Forest (KMSF) and Flambeau River SF (FRSF)

Table 3 Differences between phenological timing of curves in days-left-in-season analysis versus conventional day-of-year analysis

Species	*x*-axis	Days left in season or date when NDII = 0.2 (days)		
		FRSF mean	KMSF mean	95% CI difference in means
Black ash	DLiS	−37.6	−40.4	2.826 ± 0.098
	DATE	261.7	271.1	9.416 ± 0.077
White ash	DLiS	−26.9	−27.5	0.533 ± 0.113
	DATE	272.9	291.0	18.104 ± 0.062
Sugar maple	DLiS	−26.0	−24.3	1.655 ± 0.092
	DATE	273.0	292.5	19.520 ± 0.040
Red maple	DLiS	−28.4	−28.2	0.214 ± 0.106
	DATE	269.7	289.0	19.330 ± 0.082

Values shown are the date or days-left-in-season when the modeled NDII = 0.2; $P < 0.001$ in all cases

senescence occurs more rapidly in the south (Table 5). Using the bootstrap replicates, an unpaired, two-sided t-test for each species shows that the mean interquartile ranges are significantly greater in the north than in the south, for both the DLiS and day-of-year comparisons, indicating that these species take longer to senesce in northern study area. The difference in senescence duration when using DLiS comparisons is approximately 14 days for black ash, 11 for white ash, 12 for red maple, and 10 for sugar maple. The difference in duration of senescence was reduced but still present in the day-of-year analysis: 4 days for black ash, 7 for white ash, 3 for sugar maple, and 6 for red maple.

Comparisons among species

Senescence of black ash begins earliest in northern lowland forest stands in FRSF, followed by yellow birch (*Betula alleghaniensis*), then red maple (Fig. 6a). Tamarack (*Larix laricina*) begins to drop its leaves later than the broadleaved deciduous trees. Minimum and maximum NDII are similar for the broadleaved species, while tamarack's minimum and maximum are lower and higher, respectively. The inflection point of each species is significantly different using Tukey's HSD (Fig. 6e).

In the northern upland forest stands in FRSF differences between species are less distinct. Trembling aspen (*Populus tremuloides*) is the first species to begin senescence (Fig. 6b). The rate of senescence of aspen is comparatively slower than that of white ash or sugar maple. White ash and sugar maple reach their NDII minima before trembling aspen. White ash

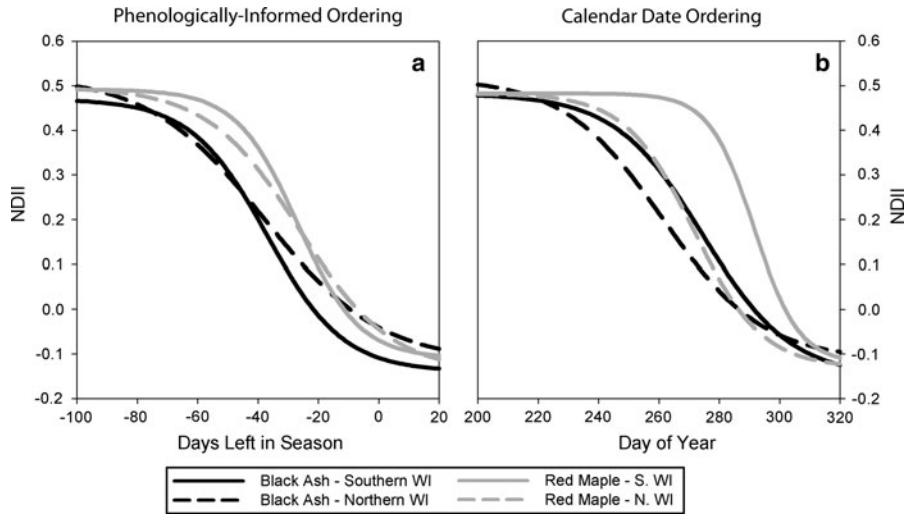

Fig. 5 Modeled curves using phenologically-informed ordering (**a**) and calendar date (**b**)

Table 4 Differences in modeled slope (β_3)of autumn senescence in selected species (df = 1998, $P < 0.001$ in all cases)

Species	Area	Mean	Std Dev	95% CI difference in means
Black ash	FRSF	−0.052	0.004	0.0249 ± 0.0005
	KMSF	−0.077	0.007	
White ash	FRSF	−0.072	0.010	0.0375 ± 0.0023
	KMSF	−0.110	0.036	
Sugar maple	FRSF	−0.071	0.007	0.0308 ± 0.0007
	KMSF	−0.101	0.008	
Red maple	FRSF	−0.066	0.005	0.0352 ± 0.0007
	KMSF	−0.101	0.011	

Table 5 Difference in senescence duration (inter-quartile range) within species between northern (FRSF) and southern (KMSF) Wisconsin, and between days-left-in-season organization versus Landsat image date organization (DATE)

Species	x-axis	FRSF mean	KMSF mean	95% CI difference in means
Black ash	DLiS	42.5	28.8	13.69 ± 0.25
	DATE	36.6	32.3	4.24 ± 0.21
White ash	DLiS	30.9	20.4	10.55 ± 0.28
	DATE	17.8	10.8	6.97 ± 0.34
Sugar maple	DLiS	31.4	21.8	9.61 ± 0.22
	DATE	13.4	10.3	3.18 ± 0.43
Red maple	DLiS	33.7	22.1	11.70 ± 0.22
	DATE	24.7	18.4	6.29 ± 0.28

Values shown are the number of days it takes to progress from 75% of NDII amplitude to 25% of NDII amplitude; for all comparisons, $P < 0.001$, df > 1000

begins and completes senescence prior to sugar maple, although there is very little difference in the patterns of senescence of the two species, and the inflection point is not significantly different.

Lowland forest stands in the southern study (KMSF) area are characterized by four locally abundant species: black ash, green ash (*F. pennsylvanica*), red maple, and silver maple (*A. saccharinum*) (Fig. 6c). Both ash species in this area begin senescence 10–15 days earlier than their maple counterparts, and the difference in timing between species is significant. Black ash starts to senesce slightly later than green ash, while red maple is slightly later than silver maple. Silver maple senesces more rapidly than the other species.

In the southern upland forest stands (KMSF) there is little variation between sugar maple, white ash, and red oak (*Quercus rubra*) (Fig. 6d). White ash senescence begins earliest, and has an inflection point significantly different from sugar maple and red oak, but the difference is slight (roughly 1–2 days) compared to the difference observed between lowland ash and lowland maple. The patterns of senescence in this area have very similar maxima and minima.

The senescence patterns of forest species in southern and northern study areas are not identical, but do overlap substantially. Generally, differences between species are consistent with the observation that all ash species in this study drop their leaves before neighboring species, but the difference is not significant for white ash in northern uplands.

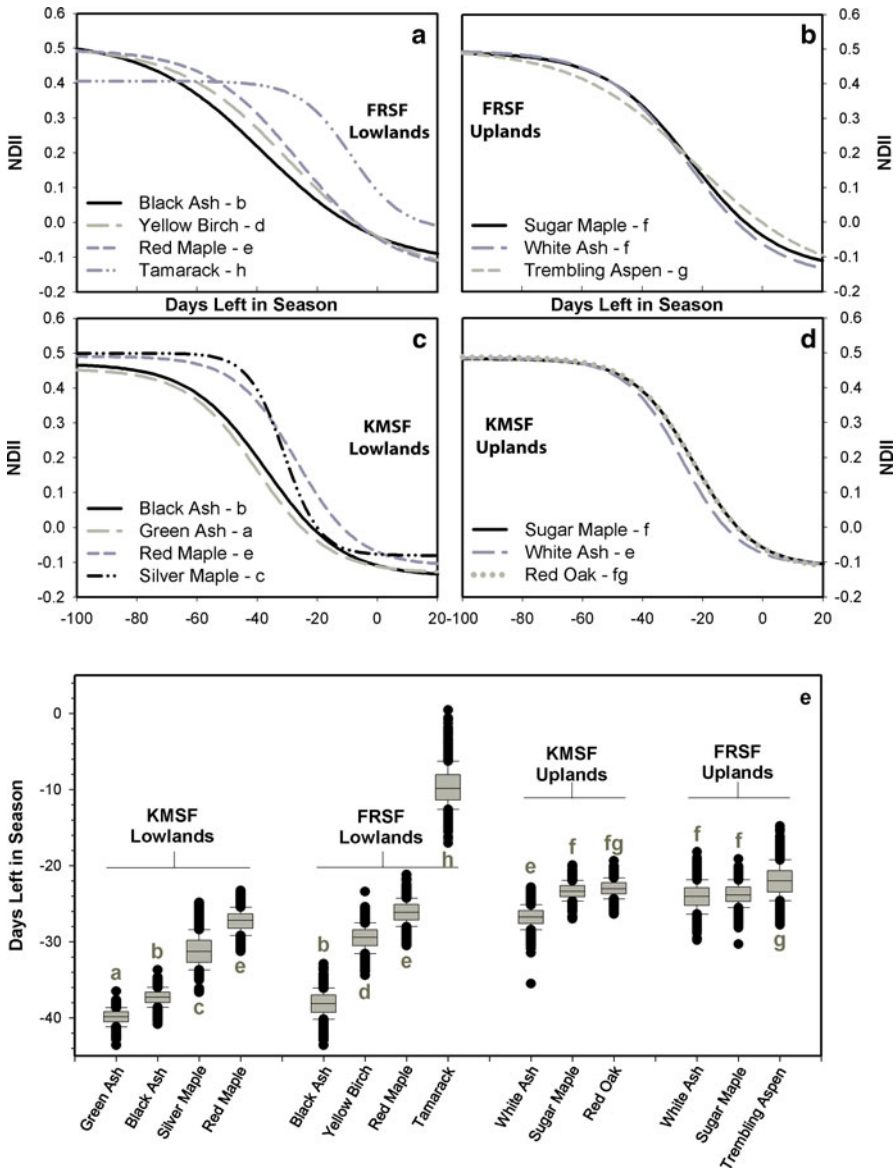

Fig. 6 Species-wise phenology in **a** lowland stands in Flambeau River State Forest (FRSF), **b** upland stands in FRSF, **c** lowland stands in Kettle Moraine SF (KMSF), **d** upland stands in KMSF. Means comparisons (**e**) using Tukey's procedure on modeled inflection points (β_4) from bootstrapped datasets for each species. *Different letters* show significant comparisons ($\alpha = 0.05$)

Discussion

Methodological considerations

The scaling method we present produces modeled patterns of senescence that are spatially and temporally comparable for prominent forest tree species in southern and northern Wisconsin. Our approach utilizes a measure of greenness (NDII) from multiple years of Landsat imagery, along with regional NACP (MODIS-derived) phenology information, to temporally align patterns of senescence (based on DLiS) between two areas that are geographically and climatically different. Alignment of the timing of senescence in different regions is necessary for comparisons of species phenology across climatically varying landscapes.

Due to interannual variability in weather and other drivers of vegetation phenology, the same calendar date in different years may not correspond to the same phenological date for a single species in a given location. As well, phenological dates within an image may be different for a single species in that image if a phenological gradient is present. Attempting to

elucidate phenological differences between species using data from multiple years and across phenological gradients without a correction for both confounds drawing insights into the traits of these species. To demonstrate this, we compared DLiS for autumn phenology to a model with day of year as the independent variable.

Our method overcame limitations evident in using calendar dates to characterize phenology when climatic gradients exist within images. While the day of year analysis confirmed that phenological timing differs by 1.5–3 weeks between northern and southern Wisconsin (Table 3; Fig. 5), our method minimized this difference for an individual species, while still demonstrating differences between species. Though there is a difference in the calendar date timing of leaf drop between study areas, DLiS accounted for much of the phenological difference caused by geographic variability by scaling those patterns with spatial estimates of broad-scale phenology. Our phenological alignment method facilitates the description and comparison of variations within species and across climatic gradients that are not obvious or apparent using day of year alone (Fig. 6), and shows that variations in land-surface phenology corresponded systematically with variations in species composition. For our purpose, DLiS represents a significant advantage over calendar-date organization of Landsat images from multiple years because the latter does not account for spatial or interannual differences in autumn phenology. These differences must be reconciled to utilize the ordered timing of species senescence in a meaningful effort to map a species across phenological gradients and to compare phenological patterns among species.

A spatially generalizable method such as this is essential to examine the relative phenological trends of species across the landscape. Fisher et al. (2006) incorporated inter-annual phenological variability into an analysis of Landsat data by scaling the images from a given year by a uniform, image-wide offset. Our method extends this approach in that we bring Landsat pixel data into phenological rather than temporal alignment, thus accounting for spatial variability of phenology within and across Landsat scenes. There are, however, limitations to our approach to consider.

The DLiS method is dependent on the depth of the satellite record. For areas where coverage is sparse, there may be too few images to produce robust results. Several approaches could increase the number of images used in the analysis, and thus strengthen the modeling:

(1) use poorer quality Landsat images (clouds, haze) with temperature or other corrections following Fisher et al. (2006) to utilize more images within the same time frame,
(2) employ synthesized Landsat-scale data from MODIS (Roy et al. 2008; Hilker et al. 2009), or,
(3) increase the range of years across which Landsat scenes are collected through the use of a different phenology product.

The disadvantages of the first two approaches include increased noise in the pixels being modeled. In the case of (2), the scale at which synthesized-image algorithms characterize phenology may be too coarse to capture fine-scale differences between species. Since synthetic images can only accommodate phenological changes observable at the MODIS scale, variations in 500 m phenology due to species composition reflect species composition at the 500 m scale, not the finer scale. This increased pixel complexity may decrease the signal from individual species, impairing performance of species-wise phenology estimates.

A different time range could also be used to increase the available images, but we were limited by the range of years in which NACP products were available (2001–2007). Use of data from a sensor system that has operated for a longer period, such as AVHRR, or the use of the full temporal span of available MODIS data would allow more fine-scale imagery to be included in the analysis. Alternative phenological scaling products do not need to be limited to satellite data; an acceptable surface could be created from appropriate ground-based climate data. Such a product would need to be region-specific, as models to predict phenology are constrained by different abiotic conditions in different regions (Jolly et al. 2005). Satellite images may be preferable to climate data for estimating phenology because they capture the actual status of the imaged vegetation.

Expansion of the time range to increase finer-scale data availability would also lean more heavily on the assumption that the vegetation community composition remained stable throughout the study period. For our purposes, i.e. examining long-lived tree species, we felt our 7 year interval to be justifiable. However,

for vegetation communities with more dynamic composition, shorter 'windows' of available fine-scale images may further constrict the data available for analysis, even with the use of alternative phenological scaling data.

Acceptable fine-scale phenological data were also scarce during the leaf-off portion of the year, due to expansive snow cover throughout the Wisconsin winter. This presented a challenge for characterization of seasonal NDII minima. NDII values increase with the presence of snow and ice (Delbart et al. 2005), so areas that receive plentiful and early snow have few leaf-off Landsat images that can be used. Exclusive use of Landsat imagery to model pixel-wise phenology resulted in poor fits for or the inability to model the leaf-off minimum portion of the curves, so we supplemented this portion of the Landsat record with NDII images calculated from snow-free MODIS images. We observed no considerable difference between leaf-off NDII derived from coincident Landsat (median = −0.075, standard deviation = 0.071) and MODIS (median = −0.089, standard deviation = 0.058) imagery. While this represented a departure from the Landsat-scale assessment of the phenological status of each pixel, the spatial variability in vegetation NDII was greatest during senescence or during the growing season, rather than during the winter dormant period.

Phenology of species

When considered in relation to their respective plant communities, and not geography, we observed that ash species were the first to drop their leaves. However, when compared across communities, all *Fraxinus* members did not undergo senescence prior to all other species: upland-inhabiting white ash dropped its leaves at about the same time as lowland maple species, while lowland-inhabiting black and green ash dropped their leaves before all other species that we modeled. This observation, with white ash senescing early for an upland species but intermediate when considered together with lowland species, is consistent with the results of Lee et al. (2003). In most cases, however, the intrinsic nature of diverse forest communities increased the amount of overlap between species.

Species that are larger or more abundant on a site contribute comparatively more to pixel phenology. To develop our patterns of senescence by species, we weighted pixel observations by the relative basal area of a species from within a sampled stand. As a consequence, relatively pure stands of each species are critical to the accuracy of the modeling. Since pure stands are rare for many species, we did not attempt to model the phenology of scarce species, and our results for species that occurred only in moderate density in mixed forests are also affected by this issue.

For the lowlands, the phenology of the major species was less affected by plots with mixed cover because of the presence of numerous "pure" stands, yielding improved results (Tables 1, 2). In KMSF (southern) we found and measured several lowland stands where more than 50% of basal area was comprised of a single species, yielding curves with high confidence and greater separability from other species. In the FRSF (northern) lowlands the relatively pure lowland stands were dominated by either black ash or tamarack. The other two major deciduous lowland species in FRSF, red maple and yellow birch, occurred in low densities, and often in association with black ash. The phenology for these species was thus influenced by the presence of black ash, which skewed their patterns towards earlier senescence and reduced their distance from black ash. Even so, our comparison of the timing of the inflection point of autumn senescence for these species showed statistically significant differences from black ash (Fig. 6e), demonstrating that the phenology of lowland ash is separable from that of other species.

The description of the phenology of upland species in both the southern (KMSF) and northern (FRSF) also showed the effects of mixed composition. Although sugar maple was abundant in most of the upland forests in high densities, few other species were as locally abundant, including white ash. Hence, the modeled phenology of many upland species incorporated the phenology of co-occurring species, blurring differences and making the species-wise patterns more similar (Fig. 6b, d). Identification and sampling of pure stands of the species of interest would achieve the sharpest delineation of species-level phenology, although such stands may be difficult to locate since most natural deciduous forests are comprised of a mix of species.

Future efforts to improve upon the characterization of the phenology of individual species will benefit from field observation of stands with nearly-pure

composition for the species of interest. This would improve the resolution of differences between the phenologies of different species, although the lack of such pure stands for most deciduous species will limit such an effort in practice. Alternatively, a technique such as independent component analysis (Ozdogan 2010) may elucidate species phenology from mixed-species pixels. In our case, the limited dimensionality of our models precluded this option for phenological unmixing by species-wise 'endmembers.'

Among the major species with relatively pure pixels, we observed a consistent pattern of a lengthened duration of senescence in the northern study area, both within and across species (Tables 4, 5). This contrasts with Zhang and Goldberg (2011), who observed shortened duration of fall foliage coloration with increasing latitude in the northeastern US and Canada. There are several explanations for this result, ranging from differences in image processing, to differences in plant communities, to biological processes. Some, but not all, of the difference in slopes is a consequence of artifacts from the NACP processing: although there was a longer senescence duration for DLiS organization over day-of-year, both approaches demonstrated statistically significantly longer IQRs for all species in the northern study area (Table 5).

In the case of black ash, our difference in duration is explained in part by differences in leaf-off minima between the two areas, as our definition of 'interquartile range' caused the duration of senescence to be dependent on the amplitude of the curve (e.g., species with a smaller amplitude have a narrower time interval between 25 and 75% of their NDII values, even if the slope is the same). The presence of conifers in black ash stands caused the later autumn phenology pattern to have a shallower slope for this species, as winter greenness in these stands was not as low as in others. However, the difference observed for the other three species was relatively consistent, with similar amplitudes of NDII values between areas. The consistency of difference in the slope of senescence across species indicated that some other factor is responsible for the difference in the rates of senescence in the two areas.

Differences in the duration of senescence, slope, and the inflection points of the same species in both study areas reflect issues in the NACP algorithm and/or DLiS approach, which could also explain some of our difference with Zhang and Goldberg (2011). MODIS-derived phenology products are sensitive to model parameters and vary in consistency between ecoregions and in their characterization of the same region (White et al. 2009). While there are errors associated with the NACP data, those errors were either systematically constant or minimal enough to describe the same species in different areas comparably. Of the four species found in both areas, inflection points of the three that were locally abundant in both areas (black ash, red maple, sugar maple) were not significantly different within each species (Fig. 6e), suggesting that NACP end-of-season estimates had similar variation in both areas.

A longer duration of senescence at more northerly latitudes is in agreement with Dixon (1976), who observed a longer duration of leaf fall in northern latitudes (36 N vs. 55 N), but did not examine differences in leaf fall rate within a species across its range. In contrast to both Dixon (1976) and our results, which utilized only two relatively discrete locations to make this observation, Zhang and Goldberg (2011) covered a regional landscape and found different patterns. Although their results showed a latitudinal gradient in autumn color phases, there were distinct locales where phenology was driven by other landscape processes such as topography, urbanization, and proximity to large bodies of water. It may be possible that a non-latitudinal landscape phenomenon drove the differences in duration of senescence that we observed.

At a finer scale, different species may vary in the way their phenology responds to abiotic gradients. In cooler areas dormancy may occur more slowly as a result of the effect of cooler temperatures on metabolic processes (or a threshold of accumulated cooling), although models to characterize senescence that utilize cooling degree days alone do not perform as well as those that also incorporate the day of year (Richardson et al. 2006). Genetics may drive some of the differences in phenological development (Lechowicz 1984), and adaptive pressure may be responsible for species-specific leaf phenology strategies which vary in response to moisture conditions (Escudero and del Arco 1987). For comparisons within species, Tateno et al. (2005) examined the phenology of several species across an altitudinal gradient following the approach of Dixon (1976). Four of the six species that were present across the gradient took longer to senesce on the higher (drier) slope. Of note, the *Acer* and *Fraxinus* species in their study took

longer to senesce in the drier environment. Further work is needed to determine if the differences we observed were the result of species-specific responses to abiotic gradients, and if so, what the drivers for these responses are.

Once re-ordered by the MODIS-scale phenology, we observed that much of the spatial variability in the autumn phenology of deciduous forest types in Landsat data was driven by spatial variation in forest community composition. Though we observed in the field that the phenology of individual trees of the same species varied, similar to Liang and Schwartz (2009), there was sufficient separation of populations among many pixels on the landscape to show differences between species, even with intra-species variability. As ash was significantly more separable from its neighbors based on phenology alone, we feel that this method presents an opportunity to map ash abundance using phenology.

Moreover, this technique presents the opportunity to examine how fine-scale variability in land surface phenology is affected by vegetation community composition. Our method can be applied across a range of climates to facilitate 30 m-resolution regional-scale phenological analysis beyond the extent of a Landsat footprint. This generalizability is unique and valuable for investigations where the phenology of a particular taxon is important. For example, the extended phenology of invasive plants has been used to locate such species (Resaco et al. 2007), but traditional analyses depend on images with fortuitous timing to capture the phenological process of interest in the study area. Considering the within- and across-scene variability of phenology in Landsat images, our approach stands to overcome some of the limitations of image differencing for phenology-oriented studies, though successful generalization will require knowledge of the plant communities in the areas to be studied.

Conclusions

We developed a method to describe pixel-wise autumn phenology using Landsat images in a consistent manner across the landscape, and demonstrated differences in end of season phenology between species that remained consistent geographically with respect to co-occurring species. Fine scale variations in autumn vegetation community phenology were driven by species composition. Our method can be extended to other ecosystems to model senescence in systems with species that exhibit unique phenology. In our case, we believe that these results provide the basis to map ash trees across a broad spatial extent (several Landsat scenes) at 30 m resolution, having shown that lowland ash species senesce significantly earlier than other deciduous forest species in Wisconsin, USA. Moreover, better understanding and discrimination of species-level phenology—temporally and spatially—could improve other landscape-level analyses of ecosystem function. The use of alternative spatial phenological products other than NACP data would increase potential applications of the DLiS method, likely overcoming issues with data-limitation.

Acknowledgments This research was funded by the Wisconsin Department of Natural Resources. Two anonymous reviewers provided feedback that greatly improved the manuscript. The authors would like to thank Jane Cummings-Carlson for collaborative support, Aditya Singh for discussion and computing support, Clayton Kingdon for help with editing and image processing, Peter Wolter for in-depth discussions, and Suming Jin for processing insights. Thanks also to Kelly Doyle, Jennifer Limbach, and Angelique Edgerton, and Nathan Rehberg for field assistance. Finally, we would like to thank the USGS for opening the Landsat data archive.

References

Ahl DE, Gower ST, Burrows SN et al (2006) Monitoring spring canopy phenology of a deciduous broadleaf forest using MODIS. Remote Sens Environ 104:88–95

Ahlgren CE (1957) Phenological observations of nineteen native tree species in northeastern Minnesota. Ecology 38:622–628

Canty A, Ripley B (2009) Boot: bootstrap R (S-Plus) Functions. R package version 1.2, 38

Curtis JT (1959) The vegetation of Wisconsin: an ordination of plant communities. The University of Wisconsin Press, Madison

de Beurs KM, Townsend PA (2008) Estimating the effect of gypsy moth defoliation using MODIS. Remote Sens Environ 112:3983–3990

Delbart N, Kergoat L, Toan TL et al (2005) Determination of phenological dates in boreal regions using normalized difference water index. Remote Sens Environ 97:26–38

Delbart N, Picard G, Le Toan T et al (2008) Spring phenology in boreal Eurasia over a nearly century time scale. Global Change Biol 14:603–614

Dixon KR (1976) Analysis of seasonal leaf fall in north temperate deciduous forests. Oikos 27:300–306

Dymond CC, Mladenoff DJ, Radeloff VC (2002) Phenological differences in tasseled cap indices improve deciduous forest classification. Remote Sens Environ 80:460–472

Escudero A, del Arco JM (1987) Ecological significance of the phenology of leaf abscission. Oikos 49:11–14

Fisher JI, Mustard JF (2007) Cross-scalar satellite phenology from ground, Landsat, and MODIS data. Remote Sens Environ 109:261–273

Fisher JI, Mustard JF, Vadeboncoeur MA (2006) Green leaf phenology at Landsat resolution: scaling from the field to the satellite. Remote Sens Environ 100:265–279

Gao BC (1996) NDWI: a normalized difference water index for remote sensing of vegetation liquid water from space. Remote Sens Environ 58:257–266

Haack RA, Jendek E, Liu H et al (2002) The emerald ash borer: a new exotic pest in North America. Mich Ento Soc News 47:1–5

Hardisky MA, Klemas V, Smart RM (1983) The influence of soil salinity, growth form, and leaf moisture on the spectral radiance of Spartina alterniflora canopies. Photogramm Eng Remote Sens 49:77–83

Hilker T, Wulder MA, Coops NC et al (2009) Generation of dense time series synthetic Landsat data through data blending with MODIS using a spatial and temporal adaptive reflectance fusion model. Remote Sens Environ 113:1988–1999

Hwang T, Song C, Vose JM, Band LE (2011) Topography-mediated controls on local vegetation phenology estimated from MODIS vegetation index. Landscape Ecol. doi: 10.1007/s10980-011-9580-8

Jolly WM, Nemani R, Running SW (2005) A generalized, bioclimatic index to predict foliar phenology in response to climate. Global Change Biol 11:619–632

Knutson RM (1997) An 18-year study of litterfall and litter decomposition in a northeast Iowa deciduous forest. Amer Midland Naturalist 138:77–83

Kodani E, Awaya Y, Tanaka K, Matsumura N (2002) Seasonal patterns of canopy structure, biochemistry and spectral reflectance in a broad-leaved deciduous *Fagus crenata* canopy. For Ecol Mgmt 167:233–249

Kokaly RF, Despain DG, Clark RN, Livo KE (2003) Mapping vegetation in Yellowstone national park using spectral feature analysis of AVIRIS data. Remote Sens Environ 84:437–456

Lechowicz MJ (1984) Why do temperate deciduous trees leaf out at different times? Adaptation and ecology of forest communities. Amer Naturalist 124:821–842

Lee DW, O'Keefe J, Holbrook NM, Field TS (2003) Pigment dynamics and autumn leaf senescence in a New England deciduous forest, eastern USA. Ecol Research 18:677–694

Leopold A, Jones SE (1947) A phenological record for Sauk and Dane counties, Wisconsin, 1935–1945. Ecol Monogr 17: 81–122

Liang L, Schwartz MD (2009) Landscape phenology: an integrative approach to seasonal vegetation dynamics. Landscape Ecol 24:465–472

Martin ME, Newman SD, Aber JD, Congalton RG (1998) Determining forest species composition using high spectral resolution remote sensing data. Remote Sens Environ 65:249–254

Mickelson JG, Civco DL, Silander JA (1998) Delineating forest canopy species in the Northeastern United States using multi-temporal TM imagery. Photogramm Eng Remote Sens 64:891–904

Morisette JT (2009) MODIS for NACP. Goddard Space flight center, National Aeronautics and Space Administration, USA. Available from http://accweb.nascom.nasa.gov/. (Accessed Jan2010)

Ozdogan M (2010) The spatial distribution of crop types from MODIS data: temporal unmixing using independent component analysis. Remote Sens Environ 114:1190–1204

Resaco J, Hale AN, Henry MC, Gorchov DL (2007) Detecting an invasive shrub in a deciduous forest understory using late-fall Landsat sensor imagery. Int J Remote Sens 28: 3739–3745

Richardson AD, Bailey AS, Denny EG et al (2006) Phenology of a northern hardwood forest canopy. Global Change Biol 12:1174–1188

Roy DP, Ju J, Lewis P et al (2008) Multi-temporal MODIS-Landsat data fusion for relative radiometric normalization, gap filling, and prediction of Landsat data. Remote Sens Environ 112:3112–3130

Schwartz MD, Reed BC, White MA (2002) Assessing satellite-derived start-of-season measures in the coterminus USA. Int J Climatol 22:1793–1805

Stimson HC, Breshears DD, Ustin SL, Kefauver SC (2005) Spectral sensing of foliar water conditions in two co-occurring conifer species: *Pinus edulis* and *Juniperus monosperma*. Remote Sens Environ 96:108–118

Tateno R, Aikawa T, Takeda H (2005) Leaf-fall phenology along a topography-mediated environmental gradient in a cool-temperate deciduous broad-leaved forest in Japan. J For Res 10:269–274

Townsend PA (2001) Relationships between vegetation patterns and hydroperiod on the Roanoke River Floodplain, North Carolina. Plant Ecol 156:43–58

Townsend PA, Walsh SJ (2001) Remote sensing of forested wetlands: application of multitemporal and multispectral satellite imagery to determine plant community composition and structure in southeastern USA. Plant Ecol 157:129–149

White A, deBeurs KM, Didan K et al (2009) Intercomparison, interpretation, and assessment of spring phenology in North America estimated from remote sensing for 1982–2006. Global Change Biol 15:2335–2359

Williams AP, Hunt ER Jr (2002) Estimation of leafy spurge cover from hyperspectral imagery using mixture tuned matched filtering. Remote Sens Environ 82:446–456

Wolter PT, Mladenoff DJ, Host GE, Crow TR (1995) Improved Forest Classification in the Northern Lake States Using Multi-Temporal Landsat Imagery. Photogramm Eng Remote Sens 61:1129–1143

Young J, Hopkins E, Anderson L (2007) Climate Summaries by Location. Wisconsin State Climatology Office. Department of Atmospheric and Oceanic Sciences, University of Wisconsin—Madison. Available from http://www.aos.wisc.edu/~sco/. (Accessed Jan 2010)

Zhang X, Goldberg MD (2011) Monitoring fall foliage coloration dynamics using time-series satellite data. Remote Sens Environ 115:382–391